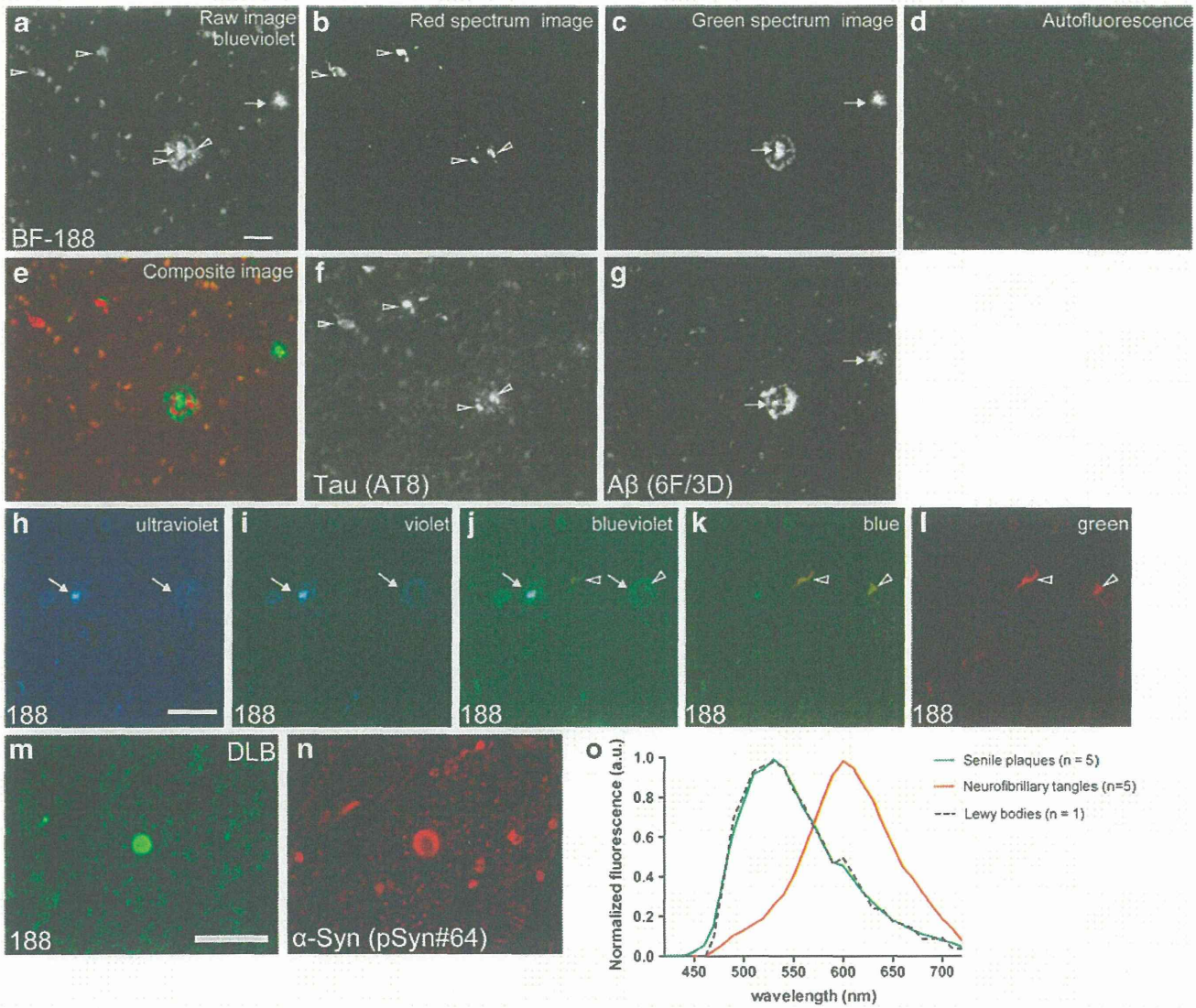

Fig. 4. Fluorescence raw image of BF-188 staining (**a**), calculated red spectrum image (**b**), and green spectrum image (**c**), autofluorescence image (**d**), and the composite image (**e**) are shown. Calculated red spectrum image was consistent with tau (AT8) immunostaining in the same section (**f**). The green spectrum image of amyloid-β immunostaining (6 F/3D) in an adjacent section (**g**) closely resembled BF-188 staining. Cored plaques were clearly and selectively visualized by BF-188 staining using ultraviolet and violet filters (**h**, **i**). They were also visualized using blue–violet filters (**j**). However, senile plaques disappear and paired helical filaments-tau was clearly and selectively visualized using blue (**k**) and green filters (**l**). Lewy bodies were also visualized by BF-188 using violet filter (**m**), which was consistent with α-synuclein immunostaining (**n**). Unmixed fluorescence spectrum of senile plaques (λ_{em}=520 nm), neurofibrillary tangles (λ_{em}=600 nm), and LBs (λ_{em}=520 nm) are shown (**o**). Scale *bars*, 50 μm.

derivatives show distinctive fluorescence spectra when bound to PHF-tau. A structure–activity-relationship study indicated that the backbone of benzimidazole was necessary to display this fluorescence property. Compared with BF-126, BF-188 has a better fluorescence property for selective detection of tau protein deposits as indicated by the larger difference between the maximum fluorescence wavelength of Aβ and PHF-tau (80 nm) for BF-188 than for BF-126 (50 nm). In fact, BF-188 clearly separated SPs from NFTs using a conventional fluorescence microscope equipped with two different excitation filter sets. Previously, a pentameric thiophene derivative, pentamer formyl thiophene acetic acid, and Nile red were reported to have similar fluorescence properties, *i.e.*, they emit different fluorescence spectra after binding to various amyloid fibrils. [4, 13]. However, these compounds are not suitable for distinguishing SPs from NFTs using MSFI, because of the small difference in their fluorescence spectra. We additionally observed the increase in fluorescence intensity of BF-188 when it binds to Aβ or tau protein aggregates (data not shown). This fluorescence property will contribute to the improvement of signal-to-background ratio in the microscopic images.

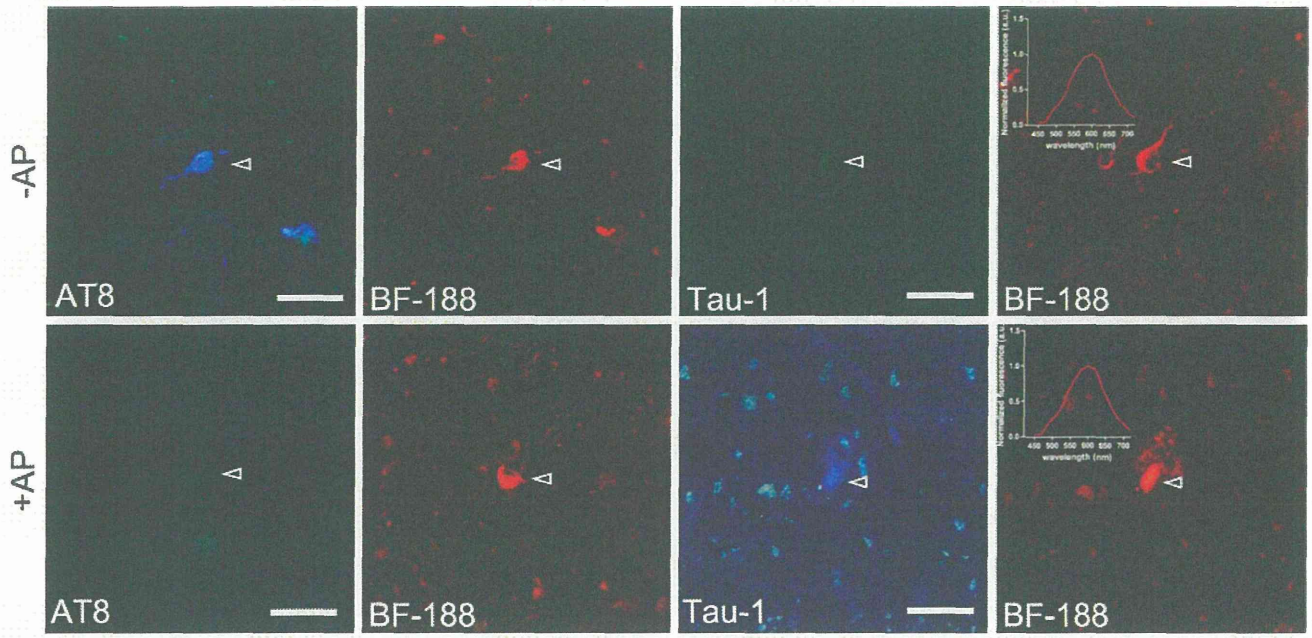

Fig. 5. Effect of tau phosphorylation on fluorescence properties of BF-188. Double staining with BF-188 and anti-tau antibody (AT8, Tau-1) was performed in Alzheimer's disease frontal brain section with or without dephosphorylation treatment. BF-188 fluorescence property was independent of tau phosphorylation. Insert notes fluorescence spectra of BF-188 excited by green filter when it was bound to neurofibrillary tangles. Scale *bars*, 50 μm.

We further investigated the mechanisms of the fluorescence spectral shift. Tau deposits, such as NFTs, neuropil threads, and dystrophic neurites, are hyperphosphorylated in AD brains [14, 15]. Thus, we hypothesized that BF-188 interacts with the phosphoric group of hyperphosphorylated tau, resulting in a red shift in emission fluorescence spectra. However, as shown in Fig. 5, the BF-188 fluorescence spectrum was independent of tau phosphorylation. LBs have also been reported to be composed of phosphorylated α-synuclein [16]. However, fluorescence spectral shift of BF-188 was not observed on α-synuclein deposits in DLB brain sections. From these findings, we think that the BF-188 fluorescence property was independent of protein phosphorylation. The BF-188 fluorescence property may depend on the conformation of pathological protein aggregates. It is speculated that the pathological conformation of α-synuclein deposits in LBs may be similar to that of Aβ deposits. We previously demonstrated that BF-227, an amyloid positron emission tomography (PET) probe, labels LBs as well as Aβ plaques in postmortem brain sections [17]. Recently, novel PET imaging tracers has been explored for *in vivo* detection of LBs in the brain of PD and DLB patients [18]. However, it is difficult to develop selective α-synuclein probe, because most of β-sheet binding compounds bind LBs as well as Aβ plaques in postmortem brain samples. These findings suggest the conformational similarity between Aβ plaques and LBs. Aβ and tau protein fibrils share the common cross-β sheet structure with 4.76 Å meridional spacing and 10.6 Å equatorial spacing [19], but the atomic structure of these protein aggregates remains elusive. Analyses using specific chemical probes will allow us to characterize the structural conformation of these pathological lessons and to better understand the structural similarity and diversity of pathological deposits in various protein misfolding diseases. Furthermore, these analyses might lead to the development of novel anti-aggregation drug.

In this study, we developed novel fluorescent probes that can selectively detect Aβ and tau deposits in a wavelength-dependent manner. These probes have the potential to be used for MSFI of the AD brain tissues. BF-188 showed a distinctive fluorescence spectrum when it was bound to NFTs. MSFI imaging with BF-188 clearly distinguished PHF-tau from Aβ in the AD brain. This technique will be an excellent tool for use to detect rapidly and selectively tau pathology as well as Aβ without the need for time-consuming immunohistochemistry. BF-188 showed sufficient brain uptake and rapid wash-out in normal mice. Thus, it can be also applied for *in vivo* monitoring of Aβ and tau deposits in the brain of mice using multiphoton microscopy, providing a better understanding of AD pathophysiology. Fluorescence probes with absorption and emission bands in the near-infrared region (600–900 nm) enables deep tissue penetration of fluorescence signals and *in vivo* detection of Aβ deposits in the brain [20]. We are currently developing long wavelength fluorescence probes for use in noninvasive MSFI.

Acknowledgment. This study was supported by the research fund from Sumitomo Electric Industries Ltd, the Small Business Innovation Research (SBIR) program of Japan, and the Grant-in-Aid for Scientific Research on Priority Areas "Integrative Brain Research" from the Ministry of Education, Culture, Sports, Science, and Technology of Japan (20019006), and Japan Society for the Promotion of Science (JSPS).

Conflict of Interest. The authors declare no competing financial interests.

Reference

1. Clinton LK, Blurton-Jones M, Myczek K et al (2010) Synergistic interactions between Abeta, tau, and alpha-synuclein: acceleration of neuropathology and cognitive decline. J Neurosci Off J Soc Neurosci 30:7281–7289
2. Zhou L, El-Deiry WS (2009) Multispectral fluorescence imaging. J Nucl Med Off Publ Soc Nucl Med 50:1563–1566
3. Ran C, Moore A (2012) Spectral unmixing imaging of wavelength-responsive fluorescent probes: an application for the real-time report of amyloid Beta species in Alzheimer's disease. Mol Imaging Biol MIB Off Publ Acad Mol Imaging 14:293–300
4. Mishra R, Sjolander D, Hammarstrom P (2011) Spectroscopic characterization of diverse amyloid fibrils *in vitro* by the fluorescent dye Nile red. Mol Biosyst 7:1232–1240
5. Okamura N, Suemoto T, Furumoto S et al (2005) Quinoline and benzimidazole derivatives: candidate probes for *in vivo* imaging of tau pathology in Alzheimer's disease. J Neurosci Off J Soc Neurosci 25:10857–10862
6. Styren SD, Hamilton RL, Styren GC, Klunk WE (2000) X-34, a fluorescent derivative of Congo red: a novel histochemical stain for Alzheimer's disease pathology. J Histochem Cytochem Off J Histochem Soc 48:1223–1232
7. Velasco A, Fraser G, Delobel P et al (2008) Detection of filamentous tau inclusions by the fluorescent Congo red derivative FSB [(trans, trans)-1-fluoro-2,5-bis(3-hydroxycarbonyl-4-hydroxy)styrylbenzene]. FEBS Lett 582:901–906
8. Murayama H, Shin RW, Higuchi J et al (1999) Interaction of aluminum with PHFtau in Alzheimer's disease neurofibrillary degeneration evidenced by desferrioxamine-assisted chelating autoclave method. Am J Pathol 155:877–885
9. Fodero-Tavoletti MT, Okamura N, Furumoto S et al (2011) (18)F-THK523: a novel *in vivo* tau imaging ligand for Alzheimer's disease. Brain 134:1089–1100
10. Berezin MY, Kao J, Achilefu S (2009) pH-dependent optical properties of synthetic fluorescent imidazoles. Chemistry 15:3560–3566
11. Kobayashi H, Ogawa M, Alford R et al (2010) New strategies for fluorescent probe design in medical diagnostic imaging. Chem Rev 110:2620–2640
12. Kirschner DA, Abraham C, Selkoe DJ (1986) X-ray diffraction from intraneuronal paired helical filaments and extraneuronal amyloid fibers in Alzheimer disease indicates cross-beta conformation. Proc Natl Acad Sci U S A 83:503–507
13. Aslund A, Sigurdson CJ, Klingstedt T et al (2009) Novel pentameric thiophene derivatives for *in vitro* and *in vivo* optical imaging of a plethora of protein aggregates in cerebral amyloidoses. ACS Chem Biol 4:673–684
14. Grundke-Iqbal I, Iqbal K, Quinlan M et al (1986) Microtubule-associated protein tau. A component of Alzheimer paired helical filaments. J Biol Chem 261:6084–6089
15. Grundke-Iqbal I, Iqbal K, Tung YC et al (1986) Abnormal phosphorylation of the microtubule-associated protein tau (tau) in Alzheimer cytoskeletal pathology. Proc Natl Acad Sci U S A 83:4913–4917
16. Fujiwara H, Hasegawa M, Dohmae N et al (2002) alpha-Synuclein is phosphorylated in synucleinopathy lesions. Nat Cell Biol 4:160–164
17. Fodero-Tavoletti MT, Mulligan RS, Okamura N et al (2009) *In vitro* characterisation of BF227 binding to alpha-synuclein/Lewy bodies. Eur J Pharmacol 617:54–58
18. Neal KL, Shakerdge NB, Hou SS, et al. (2013) Development and screening of contrast agents for *in vivo* imaging of Parkinson's disease. Molecular imaging and biology: MIB: the Official pPublication of the Academy of Molecular Imaging
19. Berriman J, Serpell LC, Oberg KA et al (2003) Tau filaments from human brain and from *in vitro* assembly of recombinant protein show cross-beta structure. Proc Natl Acad Sci U S A 100:9034–9038
20. Okamura N, Mori M, Furumoto S et al (2011) *In vivo* detection of amyloid plaques in the mouse brain using the near-infrared fluorescence probe THK-265. J Alzheimers Dis JAD 23:37–48

MOLECULAR IMAGING AND BIOLOGY

Mol Imaging Biol (2013) 15:497–506
DOI: 10.1007/s11307-012-0608-5

Published Online: 30 January 2013

World Molecular Imaging Society

RESEARCH ARTICLE

A ^{18}F-Labeled BF-227 Derivative as a Potential Radioligand for Imaging Dense Amyloid Plaques by Positron Emission Tomography

Shozo Furumoto,[1,2] Nobuyuki Okamura,[1] Katsutoshi Furukawa,[3] Manabu Tashiro,[4] Yoichi Ishikawa,[2] Kentaro Sugi,[1] Naoki Tomita,[3] Masaaki Waragai,[3] Ryuichi Harada,[1] Tetsuro Tago,[2] Ren Iwata,[2] Kazuhiko Yanai,[1] Hiroyuki Arai,[3] Yukitsuka Kudo[5]

[1]*Department of Pharmacology, Tohoku University School of Medicine, 2-1 Seiryo-machi, Aoba-ku, Sendai 980-8575, Japan*
[2]*Division of Radiopharmaceutical Chemistry, Cyclotron and Radioisotope Center, Tohoku University, Sendai, Japan*
[3]*Department of Geriatrics and Gerontology, Division of Brain Sciences, Institute of Development, Aging and Cancer, Tohoku University, Sendai, Japan*
[4]*Division of Cyclotron Nuclear Medicine, Cyclotron and Radioisotope Center, Tohoku University, Sendai, Japan*
[5]*Clinical Research, Innovation and Education Center, Tohoku University Hospital, Sendai, Japan*

Abstract

Purpose: The aims of this study were to evaluate the binding and pharmacokinetics of novel ^{18}F-labeled ethenyl-benzoxazole derivatives (i.e., [^{18}F] fluorinated amyloid imaging compound of Tohoku university ([^{18}F]FACT)) as amyloid positron emission tomography (PET) tracers and to assess [^{18}F]FACT efficacy in imaging of Alzheimer's disease (AD).

Procedures: Binding assay was conducted using synthetic amyloid-β (Aβ) fibrils, fluorescence microscopy, and autoradiogram in three postmortem AD brains. Pharmacokinetics of [^{18}F]FACT was assessed using 12 Crj:CD-1 (ICR) mice. *In vivo* binding ability with brain amyloid was investigated using amyloid precursor protein (APP) transgenic mouse. Clinical PET scanning using [^{18}F]FACT was performed in ten healthy controls and ten mild cognitive impairment and ten AD patients.

Results: [^{18}F]FACT showed high binding affinity for synthetic Aβ fibrils, preferential binding to dense cored plaques in brain sections, and excellent brain uptake and rapid clearance in mice. Injection in APP mice resulted in specific *in vivo* labeling of amyloid deposits in the brain. PET scans of AD patients showed significantly higher [^{18}F]FACT uptake in the neocortex compared to controls ($P<0.05$, Kruskal–Wallis test).

Conclusion: [^{18}F]FACT is a promising agent for imaging dense Aβ plaques in AD.

Key words: Alzheimer's disease, Amyloid, Early diagnosis, Positron emission tomography

Introduction

Alzheimer's disease (AD) is an age-dependent and irreversible neurodegenerative disorder leading to deterioration of memory and cognitive function. Although the exact mechanisms underlying pathogenesis of AD are not fully understood, formation of brain amyloid plaques through aggregation and deposition of amyloid-β protein (Aβ) is considered to be the initial pathogenic event that may precede the appearance of clinical AD symptoms by decades. Recently, new criteria for diagnosing AD were proposed by the National Institute on Aging—Alzheimer's Association workgroups [1]. The new diagnostic criteria include the use of biomarkers for amyloid deposition to aid

Correspondence to: Nobuyuki Okamura; *e-mail:* nookamura@med.tohoku.ac.jp

in diagnosis of AD. Thus, *in vivo* detection of amyloid depositions with positron emission tomography (PET) has received much attention as a potential technology for early or presymptomatic diagnosis of AD. For this purpose, a number of radiotracers for Aβ aggregates have been synthesized and evaluated as candidates for PET amyloid imaging agents, and some of these are undergoing clinical investigation [2–4].

Among them, *N*-methyl-[^{11}C]-2-(4′-methylaminophenyl)-6-hydroxybenzothiazole ([^{11}C]Pittsburgh compound B, [^{11}C]PiB) is currently the most widely used in clinical research [5]. Labeling of PET tracers with ^{18}F ($T_{1/2}$= 109.8 min) allows time for their delivery to numerous PET centers and contributes to spreading their use. Several ^{18}F-labeled amyloid PET tracers, including [^{18}F]flutemetamol, [^{18}F]florbetaben, [^{18}F]florbetapir, and [^{18}F]AZD4694, have been developed, and to date, [^{18}F]florbetapir has become commercially available [6–9]. An increasing number of PET studies in humans have clearly demonstrated that amyloid PET is a potentially useful technique to visualize and quantify the distribution of Aβ plaques of AD patients [5]. In addition, a proportion of elderly normal subjects present with [^{11}C]PiB retention in the neocortex [10–12], suggesting that amyloid PET is potentially useful for presymptomatic detection of Aβ pathology. Although neocortical PiB retention is considered as a high risk for future cognitive decline, not all PiB-positive normal individuals are destined to develop dementia. Some additional biomarkers are thus necessary for accurate prediction of future conversion to dementia. According to previous histopathological study, progression to dementia is associated with a shift from non-fibrillar to fibrillar amyloid deposits in the brain [13]. Thus, selective detection of dense fibrillar amyloid might be advantageous for predicting progression to dementia.

Previously, we had succeeded in developing a unique scaffold of a radioligand, [^{11}C]2-(2-[2-dimethylaminothiazol-5-yl]ethenyl)-6-(2-[fluoro]ethoxy)benzoxazole ([^{11}C]BF-227), as an amyloid imaging probe [3, 14]. Our previous study demonstrated that Aβ deposits in AD patients can be clearly detected by [^{11}C]BF-227 PET [15]. Neocortical [^{11}C]BF-227 retention was further observed in subjects with mild cognitive impairment (MCI) [16]. Using [^{11}C]BF-227 PET, we achieved a sensitivity of 100 % and a specificity of 71.4 % in distinguishing MCI converters to AD from MCI non-converters [17], suggesting the usefulness of this radiotracer for accurate prediction of future progression to dementia. To further take advantage of this imaging potential, especially in a large clinical study, we anticipated that a ^{18}F-labeled derivative of BF-227 would be valuable due to the longer half-life of ^{18}F compared with ^{11}C.

In this study, we performed a biological evaluation of a series of ^{18}F-labeled 2-ethenyl-benzoxazole derivatives (Fig. 1) to select a candidate for clinical application. The one selected, [^{18}F]Fluorinated Amyloid Imaging Compound of Tohoku University ([^{18}F]FACT), was further evaluated for its binding characteristics with Aβ fibrils and plaques and then for its clinical utility as a probe for imaging amyloid in AD.

Methods

Radiosynthesis of ^{18}F-Labeled 2-Ethenyl-Benzoxazole Derivatives

The chemical structures of the 2-ethenyl-benzoxazole derivatives are summarized in Fig. 1. The compounds and their precursors for ^{18}F-labeling were synthesized according to the method described previously [18]. ^{18}F-labeled compounds were prepared according to the following method. The aqueous $^{18}F^-$ contained in K_2CO_3 solution (1.27 to 3.28 GBq) and Kryptofix 2.2.2 were put into a brown vial, and then the water was azeotropically removed with acetonitrile by heating at 110 °C and He-gas flow. After drying, the activated [^{18}F]KF/Kryptofix 2.2.2. was reacted with a tosylate precursor in dimethyl sulfoxide (DMSO) at 110 °C for 10 min, followed by addition of water to quench. The product was extracted by solid-phase extraction with Sep-Pak ^{t}C18 cartridge (Waters) and then eluted with ethanol. The ^{18}F-labeled compound was separated from the eluent by semi-preparative reversed-phase high-performance liquid chromatography (RP-HPLC), isolated from the collected fraction by solid-phase extraction with Sep-Pak ^{t}C18

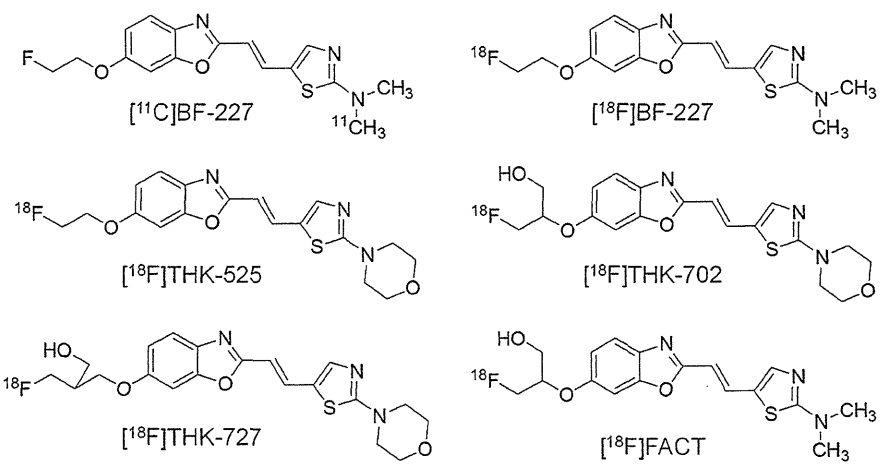

Fig. 1. Chemical structures of [^{11}C]BF-227 and its ^{18}F-labeled 2-ethenyl benzoxazole derivatives.

cartridge, and finally dissolved in DMSO or saline with polysorbate-80 (<0.1 %) for biological evaluation.

[^{11}C]BF-227 was synthesized from the precursor by *N*-methylation with [^{11}C]methyl triflate in DMSO and separated from the crude mixture by semi-preparative RP-HPLC, as described previously [15]. The purified [^{18}F]FACT and [^{11}C]BF-227 were solubilized in isotonic saline containing 1 % polysorbate-80 and 5 % ascorbic acid and then filter-sterilized with 0.22 μm Millipore filter for clinical use.

Fluorescent Staining

Postmortem brain tissue from a 69-year-old man with autopsy-confirmed AD was obtained from Fukushimura Hospital (Toyohashi, Japan). Experiments were performed under the regulations of the hospital ethics committee. Serial sections (6 μm) taken from paraffin-embedded blocks of the temporal cortex were prepared in xylene and ethanol. Before staining with test compounds, quenching of autofluorescence was performed. The quenched tissue section was immersed in 100 μM of test compounds containing 50 % ethanol for 10 min. The stained section was then dipped briefly into water before coverslipping with FluorSave Reagent (Calbiochem, La Jolla, CA, USA) and examination using an Eclipse E800 microscope (Nikon, Tokyo, Japan) equipped with a V-2A filter set (excitation 380 to 420 nm, dichroic mirror 430 nm, long pass filter 450 nm). An adjacent section was immunostained using 4G8 (Signet, Dedham, MA, USA), a monoclonal antibody against Aβ. After pretreatment with 90 % formic acid for 5 min, sections were immersed in blocking solution for 30 min and then incubated for 60 min at 37 °C with 4G8 at a dilution of 1:100. After incubation, sections were processed with biotinylated anti-mouse IgG (Wako) for 60 min, followed by Texas Red-conjugated streptavidin (Vector Laboratories, Burlingame, CA, USA).

In Vitro Autoradiography

A temporal brain section from a 76-year-old female AD patient was incubated with 1.85 MBq/ml of [^{18}F]FACT at room temperature for 20 min and then washed briefly with water and 70 % ethanol. After drying, the labeled section was exposed to a BAS-III imaging plate (Fuji Film, Tokyo, Japan) for 120 min. Autoradiograms were obtained using a BAS-5000 phosphor imaging instrument (Fuji Film, Tokyo, Japan). Neighboring sections were immunostained using 4G8 anti-Aβ monoclonal antibody. After incubation with 4G8, sections were processed by the avidin–biotin method using a Pathostain ABC-POD(M) Kit (Wako, Osaka, Japan) and diaminobenzidine tetrahydrochloride.

In Vitro Binding Study

Amyloid β_{1-40} (Peptide Institute, Inc., Japan) was dissolved in 50 mM potassium phosphate buffer (pH 7.4) to a final concentration of 20 μM. To prepare amyloid fibrils, the solution was incubated at 37 °C for 4 days at 85 rpm and then sonicated to obtain a uniform suspension. The fibril solution was diluted to 2 μM with phosphate-buffered saline (PBS) containing 0.1 % bovine serum albumin (BSA). For saturation binding assay, 100 μl of the fibril solution was mixed with [^{18}F]FACT solution (0.2 to 800 nM, PBS containing 0.1 % BSA and 2 % DMSO, 100 μl) in a 96-well plate. Non-specific binding was defined in the presence of 2 μM FACT in the final solution. The mixture was incubated for 40 min at room temperature and then was passed through the glass filter plate under vacuum with MultiScreen HTS Vacuum Manifold (Millipore Corp., USA), followed by washing with PBS containing 0.1 % BSA twice. Radioactivity of the filter was counted with an automatic gamma counter. The binding data were analyzed with curve-fitting software that calculates the K_d and B_{max} using non-linear regression (GraphPad Prism Version 5.0, GraphPad Software, San Diego, CA, USA).

Biodistribution Study in Normal Mice

The experimental protocols were reviewed by the Committee on the Ethics of Animal Experiments at Tohoku University School of Medicine and performed in accordance with the Guidelines for Animal Experiments issued by the Tohoku University School of Medicine. Male Crj:CD-1 (ICR) mice (6 weeks old, 25 to 30 g, n=12) were injected in a lateral tail vein with ^{18}F-labeled test compounds (370 to 740 kBq) contained in isotonic saline (0.2 ml). The mice were sacrificed by cervical dislocation following heart puncture to obtain blood samples at 2, 30, and 60 min postinjection (n=4 at each time point). Tissues of interest were excised and weighed, and the radioactivity was counted in an automatic gamma-counter. Radioactivity uptake data are expressed as percent of injected dose per gram of tissue (%ID/g).

Autoradiography of Aβ Deposits in Living Transgenic Mice

An amyloid precursor protein (APP) transgenic (Tg) mouse (female, 31 months old) and a wild-type littermate (female, 31 months old) were injected with [^{18}F]FACT (37 MBq) *via* tail vein. The mice were sacrificed by cervical dislocation at 2 h postinjection, and the brains were rapidly excised and frozen in liquid nitrogen. Frozen sections of 20 μm thick were prepared from the brains for *ex vivo* autoradiography. Autoradiograms were obtained in the same manner described above. The sections used for autoradiography were then subjected to fluorescent staining with thioflavin-S according to the previously described method [19].

Clinical PET Study Using [^{18}F]FACT

Ten patients with amnestic MCI, ten patients with AD, and ten normal age-matched controls participated in the clinical PET study using [^{18}F]FACT. Please refer to Table 1 for characteristics of participants. [^{11}C]BF-227 PET scan was additionally performed in two patients with AD (70-year-old woman (MMSE score 17) and 79-year-old man (MMSE score 20)) and 1 normal control subject (60-year-old man (MMSE score 30)). The average time interval between [^{18}F]FACT and [^{11}C]BF-227 PET scans was 12±6 months. Diagnosis of probable AD was based on criteria from the National Institute of Neurological and Communicative Disorders and Stroke and the Alzheimer's Disease Related Disorders Association [20]. The diagnosis of amnestic MCI was made according to published criteria described previously [21]. The control subjects were

Table 1. Subject and patient demographics in [^{18}F]FACT PET comparisons

	NC	MCI	AD
N	10	10	10
Gender (F/M)	4/6	7/3	7/3
Age (years)	69.8±8.8 (60–89)	74.2±8.8 (57–89)	74.5±4.6 (66–81)
MMSE score	29.9±0.3 (29–30)	26.4±1.1 (24–28)	19.8±3.0 (15–24)

recruited from volunteers who were taking no centrally acting medications, had no cognitive impairment, and had no cerebrovascular lesions, including asymptomatic cerebral infarction on T2-weighted studies, identified *via* MRI. All volunteers were screened using a questionnaire and medical history, and those with medical conditions potentially affecting the central nervous system were excluded. The Committee on Clinical Investigation at Tohoku University School of Medicine and the Advisory Committee on Radioactive Substances at Tohoku University approved the study protocol. After complete description of the study to the patients and subjects, written informed consent was obtained.

Image Acquisition Protocols

[^{18}F]FACT-PET and [^{11}C]BF-227-PET study was performed using a SET-2400W PET scanner (Shimadzu, Kyoto, Japan). After intravenous injection of 111–185 MBq of [^{18}F]FACT or 211–366 MBq of [^{11}C]BF-227, dynamic PET images were obtained for 60 min (23 sequential scans; 5 scans×30 s, 5 scans×60 s, 5 scans×150 s, and 8 scans×300 s) with the subject's eyes closed. SUV summation images at 0–10, 10–20, 20–30, 30–40, 40–50, and 50–60 min postinjection were created for the analysis of tracer uptake. T1-weighted MR images were obtained using a SIGNA 1.5 T machine (General Electric, Milwaukee, WI, USA).

Image Analysis

Firstly, standardized uptake value (SUV) images of [^{18}F]FACT and [^{11}C]BF-227 were obtained by normalizing tissue radioactivity concentration by injected dose and body weight. Subsequently, individual MR images were anatomically coregistered into individual PET images using Statistical Parametric Mapping software (SPM5: Welcome Department, UK). Regions of interest (ROIs) were placed on individual axial MR images in the cerebellar hemisphere, frontal cortex [Brodmann's areas (BA) 8, 9, 10, 44, 45, 46, and 47], lateral temporal cortex (BA 21, 22, 37, and 38), parietal cortex (BA 39 and 40), occipital cortex (BA 17), anterior cingulate cortex, posterior cingulate cortex, medial temporal cortex (BA 27, 28, 34, and 35), striatum, pons, and subcortical white matter, as described previously [15]. The ROI information was then copied onto dynamic PET SUV images, and regional SUVs were sampled using PMOD software (PMOD Technologies, Ltd., Zurich, Switzerland). The ratio of regional SUV to cerebellar SUV (SUVR) was calculated as an index of tracer retention. Averaged SUVR in the frontal, temporal, parietal, and posterior cingulate cortices was considered representative of tracer retention in the neocortex (neocortical SUVR). The inter-rater reliability for the ROI measurement was tested between two raters (N.O. and K.S.) in seven subjects and patients. The intra-class correlation coefficient was 0.95.

Statistical Analysis

For statistical comparison in the three groups, we applied the Kruskal–Wallis test followed by Dunn's multiple comparison test. Differences of time activity curves (TACs) in [^{18}F]FACT PET were also evaluated by repeated measures ANOVA followed by the Bonferroni–Dunn post hoc test. For statistical comparisons of PET measurements in control and AD groups, we used the Mann–Whitney *U* test. Effect size coefficients (Cohen's *d*) were also calculated for the evaluation of group differences in PET measurements. Statistical significance for each analysis was defined as $P<0.05$. Correlations between [^{18}F]FACT and [^{11}C]BF-227 SUVR in the frontal, temporal, parietal, and occipital cortices of three subjects (two AD and one normal control) were determined using Pearson's correlations. A linear model was applied to the data to obtain a correlation coefficient and *p* value. These analyses were performed using GraphPad Prism5 software (GraphPad, San Diego, CA, USA).

Results

Radiosynthesis

^{18}F-labeled 2-ethenyl-benzoxazole derivatives (Fig. 1) were obtained in yields of 32 % on average (21 to 44 %, decay-corrected) with radiochemical purity greater than 99 % after HPLC purification. The specific activities ranged 70 to 180 GBq/μmol, corrected at the end of synthesis.

In Vitro Binding to Aβ Plaques in AD Brain Sections

Binding ability of 2-ethenyl-benzoxazole derivatives to Aβ plaques was examined using AD brain sections from a 69-year-old man with autopsy-confirmed AD. As shown in Fig. 2a, c, dense cored plaques (arrowheads) were clearly stained with FACT. In particular, Aβ plaque cores were brightly stained with this compound. The fluorescent staining pattern of FACT correlated well with Aβ immunostaining (Fig. 2b) and thioflavin-S staining (Fig. 2d) in adjacent sections. Other compounds produced similar results in the histopathological staining of AD brain sections from a 69-year-old man with autopsy-confirmed AD.

In vitro autoradiography at tracer dose indicated [^{18}F] FACT binding to dense Aβ deposits (arrowheads) in AD temporal brain sections from a 76-year-old female AD patient (Fig. 2e–h). Tracer signals were additionally detected

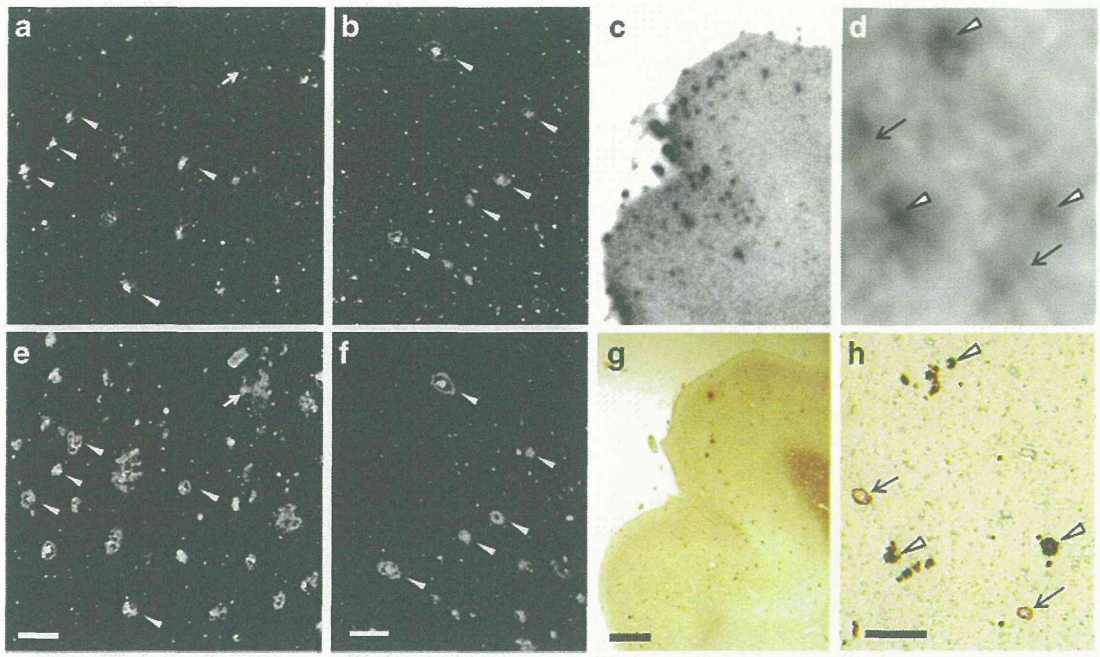

Fig. 2. **a–d** Fluorescence microscopy images of AD brain sections from a 69-year-old man with autopsy-confirmed AD stained with FACT (**a**, **c**), anti-Aβ (4 G8) antibody (**b**), and thioflavin-S (**d**). *Arrowheads* delineate dense cored plaques, respectively. **e–h** Autoradiogram of AD brain section from a 76-year-old female AD patient with [^{18}F]FACT (**e**, **g**) and images of the adjacent section immunostained with anti-Aβ (4 G8) antibody (**f**, **h**). *Arrows* and *arrowheads* delineate congophilic amyloid angiopathy and dense cored plaques, respectively. *Bars* 100 μm (**a–d**), 2 mm (**e–f**), 200 μm (**g–h**).

in congophilic amyloid angiopathy (arrows). These results indicated that FACT and its derivatives had an ability to detect pathological dense Aβ deposits in AD brain tissue.

Binding Affinity to Synthetic Aβ Fibrils

Binding properties of [^{18}F]FACT with Aβ fibrils were investigated by *in vitro* binding assay. Scatchard analysis of FACT binding to Aβ fibrils showed two classes of binding sites: a high-affinity site (K_d=9.4 nM; B_{max}= 0.16 pmol/nmol of Aβ) and a low-affinity site (K_d= 263 nM; B_{max}=1.52 pmol/nmol of Aβ).

Biodistribution Study in Normal Mice

Two important properties of an amyloid imaging probe are rapid brain uptake and rapid clearance from the normal brain without non-specific binding. These properties of the ^{18}F-labeled 2-ethenyl-benzoxazole derivatives were evaluated by biodistribution studies in 12 normal mice (n=4 at each time point). The radioactivity uptake in the blood, brain, liver, kidney, and bone is summarized in Table 2. Regarding brain uptake, all of the ^{18}F-labeled derivatives showed rapid and sufficient brain uptake (4 to 6 %ID/g at 2 min) and smooth washout after that. However, the brain uptake at 60 min varied from 0.28 to 1.68 %ID/g, suggesting a different clearance property in normal brain. Among the derivatives, [^{18}F]FACT indicated the highest ratio of brain uptakes at 2 min to that at 60 min (4.64/0.28=16.6). Additionally, mice injected with [^{18}F]FACT exhibited no increase of the radioactivity uptake in bone with time, unlike with [^{18}F]BF-227, suggesting that [^{18}F] FACT has good stability in regard to metabolic defluorination *in vivo*. Thus, we selected [^{18}F]FACT as the candidate for the clinical comparisons.

Autoradiography of Aβ Deposits in Living Transgenic Mouse

In vivo binding ability of [^{18}F]FACT with amyloid plaques was evaluated in the APP-Tg mouse. Autoradiographic images of the APP-Tg mouse brain post-intravenous injection of [^{18}F]FACT displayed high uptake of the labeling compound in the cortex and hippocampus (Fig. 3a). In contrast, no notable binding was observed in the brain of wild-type mouse (Fig. 3b). These [^{18}F]FACT binding results in APP-Tg mouse brain corresponded closely with those of *in vitro* thioflavin-S staining in the same brain sections (Fig. 3c, d). These results warranted further clinical investigation of [^{18}F]FACT PET in AD patients.

Clinical PET Study Using [^{18}F]FACT

Demographic data for the participants are summarized in Table 1. No statistical difference in age was observed among the three groups. MCI and AD patients had significantly lower mean MMSE scores than normal controls (P<0.05,

Table 2. Biodistribution of ^{18}F-labeled compounds in mice

Tracers	Time (min)	Radioactivity uptakes (%ID/g)				
		Blood	Brain	Liver	Kidney	Bone
[^{18}F]BF-227	2	2.93±0.08	6.05±0.45	7.97±1.59	9.63±0.89	1.59±0.27
	30	2.14±0.17	1.91±0.05	5.75±0.42	3.04±0.15	4.38±1.24
	60	2.09±0.15	1.67±0.14	5.48±0.23	2.42±0.20	7.04±0.75
[^{18}F]THK-525	2	2.82±0.38	4.73±1.32	5.93±1.40	7.72±2.44	1.77±0.87
	30	2.20±0.24	2.05±0.16	3.55±0.60	2.32±0.18	6.74±2.20
	60	1.91±0.29	1.68±0.15	2.47±0.23	1.48±0.14	9.65±0.89
[^{18}F]THK-702	2	3.34±0.13	4.15±0.28	7.53±0.50	13.6±0.88	1.95±0.34
	30	1.06±0.19	0.53±0.03	4.55±0.39	1.58±0.64	0.92±0.11
	60	0.67±0.08	0.35±0.04	3.65±0.72	0.65±0.09	1.16±0.70
[^{18}F]THK-727	2	2.94±0.33	4.06±0.26	9.89±4.16	11.4±1.35	2.08±0.39
	30	1.52±0.10	1.04±0.08	6.68±1.22	2.47±0.36	6.61±0.79
	60	0.66±0.10	0.69±0.02	4.04±1.87	0.98±0.14	9.33±1.34
[^{18}F]FACT	2	3.65±0.66	4.64±0.55	9.38±0.43	10.2±1.05	1.84±0.18
	30	1.19±0.49	0.53±0.11	11.3±1.32	4.17±0.44	0.88±0.07
	60	0.64±0.13	0.28±0.04	14.1±0.55	3.25±0.27	1.38±0.46

Data are expressed as mean±SD (n=4 at each time point)

Kruskal–Wallis test). AD patients additionally had significantly lower mean MMSE scores than those with MCI ($P<$ 0.05, Kruskal–Wallis test). No toxic events were observed in the current clinical trial. The SUV-TACs from [^{18}F]FACT-PET in AD patients and normal control subjects are shown in Fig. 4. Both groups showed rapid entry of [^{18}F]FACT into the neocortex and cerebellum. In the AD patients, the temporal cortex, known to contain high concentrations of fibrillar amyloid plaques in AD, showed retention of [^{18}F] FACT during the later time points compared with the cerebellum (Fig. 4a). In contrast, TACs in the temporal cortex and the cerebellum were nearly identical in normal subjects (Fig. 4b). The subcortical white matter regions showed relatively lower entry and slower clearance than gray matter areas, but no difference in TACs between AD patients and normal controls.

SUVR in the lateral temporal cortex of AD patients was significantly higher over 10 min postinjection of [^{18}F]FACT than those of normal controls ($p<0.05$, Mann–Whitney U test) and reached maximum value at 30 to 40 min postinjection (Fig. 4c). Effect size between AD and normal controls showed the highest value at 30 to 40 min postinjection of [^{18}F]FACT (Table 3). The ratio of SUVR in AD to SUVR in normal controls became constant after

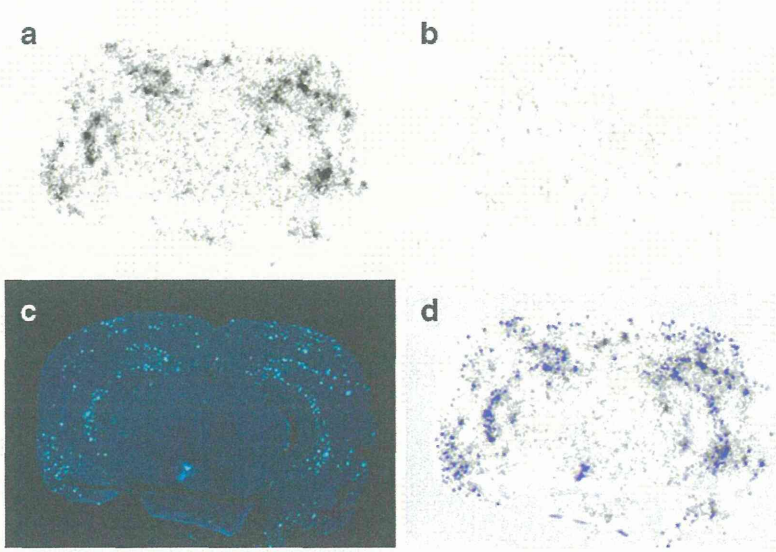

Fig. 3. *Ex vivo* autoradiograms of brain sections from APP transgenic (Tg) mouse (**a**) and wild type mouse (**b**). The brains were excised at 2 h after intravenous injection of [^{18}F]FACT. Aβ plaques in APP-Tg mouse brain were clearly stained with thioflavin-S (**c**). A merged image of **a** and **c** is shown in **d**.

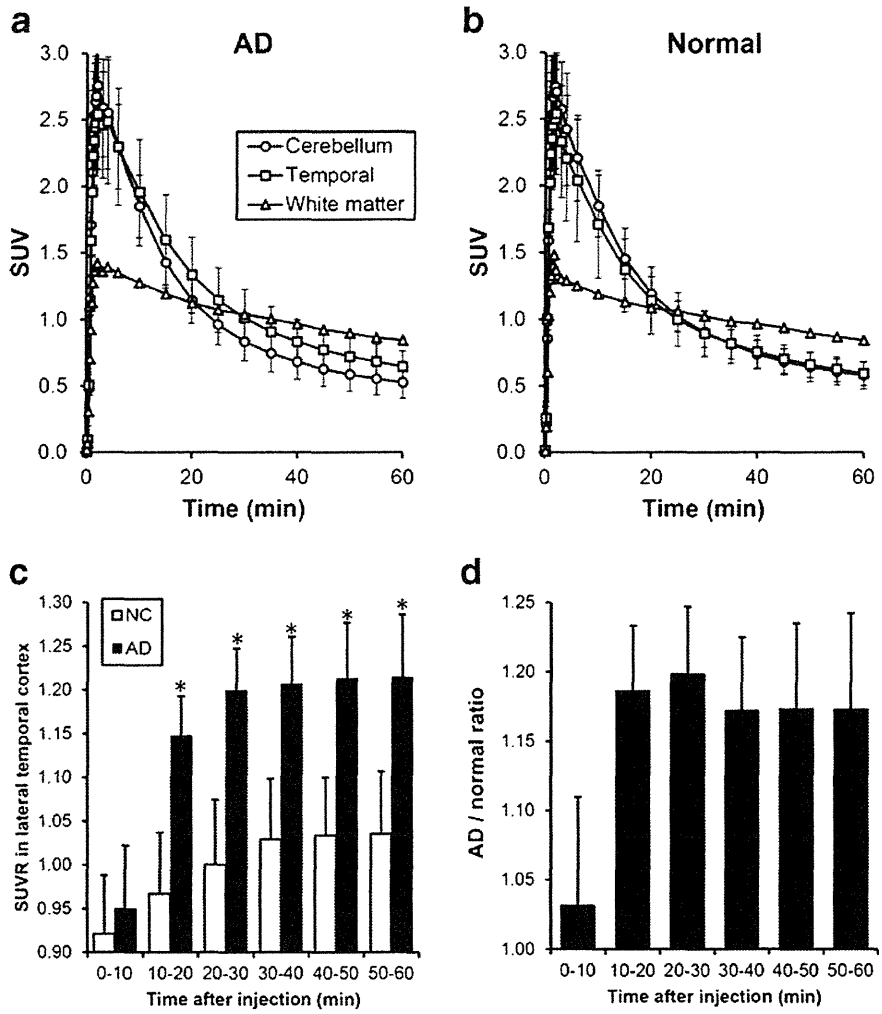

Fig. 4. Time activity data for [^{18}F]FACT PET in humans. Time activity curves of [^{18}F]FACT in ten AD patients (**a**) and ten normal controls (**b**) are shown. Each point represents the mean±standard deviations of data. Time course of [^{18}F]FACT SUVR in the lateral temporal cortex (**c**) and AD *vs* normal ratio of SUVR in the lateral temporal cortex (**d**) are also shown. *P<0.05 by the Mann–Whitney U test.

30 min (Fig. 4d). Based on these results, we selected summed dynamic images from 30 to 40 min for the ROI analysis of PET data.

SUVR images of [^{18}F]FACT for a normal control subject (a 60-year-old man, MMSE score 30) and an AD patient (70-year-old woman, MMSE score 17) are shown in Fig. 5a. Cortical retention of [^{18}F]FACT at 30 to 40 min postinjection was evident in the AD patient, as contrasted with the images of the normal control subject. This pattern of distribution was consistent with the distribution of [^{11}C]BF-227 at 30 to 40 min postinjection in the same subject and patient pair (Fig. 5a). The SUV-TACs from [^{18}F]FACT-PET were compared with those from [^{11}C]BF227-PET in the same AD patient (70-year-old woman, MMSE score 17). As shown in Fig. 5b, [^{18}F]FACT showed faster washout from both temporal cortex and cerebellum than [^{11}C]BF-227. The regional SUVR of [^{18}F]FACT at 30 to 40 min postinjection was compared with that of [^{11}C]BF-227 at the same time frame. SUVR values in the frontal, temporal, parietal, and occipital cortices of three subjects (two AD and one normal control) were used for this analysis. As shown in Fig. 5c, regional SUVR of [^{18}F]FACT were significantly correlated with that of [^{11}C]BF-227 (Pearson's r= 0.931, P<0.001) in these three subjects.

In the quantitative comparison of regional SUVR 30 to 40 min post-administration, the values for the frontal, lateral

Table 3. Time course of lateral temporal [^{18}F]FACT SUVR and effect size measures in ten normal controls and ten AD patients

Time (min)	Normal control	AD	Cohen's d
30–40	1.07±0.06	1.22±0.05*	2.67
40–50	1.08±0.06	1.23±0.06*	2.37
50–60	1.09±0.06	1.23±0.06*	2.34

*P<0.05 by the Mann–Whitney U test